C. R. Palevol 16 (2017) 521–532

Comptes Rendus Palevol

www.sciencedirect.com

Human Palaeontology and Prehistory (Palaeoanthropology)

Inner structural organization of the distal humerus in *Paranthropus* and *Homo*

Organisation de la structure interne de l'humérus distal chez Paranthropus *et* Homo

Marine Cazenave[a,b,*], José Braga[b,c], Anna Oettlé[d,a], John Francis Thackeray[c], Frikkie de Beer[e], Jakobus Hoffman[e], Metasebia Endalamaw[f], Blade Engda Redae[f], Laurent Puymerail[g], Roberto Macchiarelli[h,i]

[a] *Department of Anatomy, University of Pretoria, Pretoria, South Africa*
[b] *Computer-assisted Palaeoanthropology Team, UMR 5288 CNRS–Université Paul-Sabatier, 37, allées Jules-Guesde, 31000 Toulouse, France*
[c] *Evolutionary Studies Institute and School of Geosciences, University of the Witwatersrand, Johannesburg, South Africa*
[d] *Department of Anatomy and Histology, Sefako Makgatho Health Sciences University, Ga-Rankuwa, Pretoria, South Africa*
[e] *South African Nuclear Energy Corporation, Pelindaba, South Africa*
[f] *Authority for Research and Conservation of Cultural Heritage (ARCCH), National Museum of Ethiopia, Addis Ababa, Ethiopia*
[g] *UMR 7268 CNRS–Université d'Aix–Marseille–EFS, 13344 Marseille, France*
[h] *UMR 7194 CNRS–Muséum national d'histoire naturelle, 75013 Paris, France*
[i] *Unité de formation géosciences, Université de Poitiers, 86073 Poitiers, France*

ARTICLE INFO

Article history:
Received 27 February 2017
Accepted after revision 13 June 2017
Available online 1 August 2017

Presented by Roberto Macchiarelli and Clément Zanolli

Keywords:
Distal humerus
Inner structure
Cortical bone topography
Paranthropus
Homo

ABSTRACT

The taxonomic attribution of isolated hominin distal humeri has been a matter of uncertainty and disagreement notwithstanding their relative abundance in the fossil record. Four taxonomically-based morphotypes, respectively representing *P. boisei*, *P. robustus*, non-*erectus* early *Homo* and *H. erectus*, have been identified based on the cross-sectional outer shape variation of an assemblage of Plio-Pleistocene eastern and southern African specimens (Lague, 2015). However, the existence of possible differences between *Paranthropus* and *Homo* in the inner structural organisation at this skeletal site remains unexplored. We used noninvasive imaging techniques to tentatively characterize the endostructural organization of five early Pleistocene distal humeri from South Africa (TM 1517g, SK 24600, SKX 10924, SKX 34805) and Ethiopia (Gombore IB), which have been variably attributed to *Paranthropus* or *Homo*. While the investigated specimens reveal diverse degrees of inner preservation related to their taphonomic and diagenetic history, in all but SK 24600 from Swartkrans we could comparatively assess some geometric properties at the most distal cross-sectional level (%CA, I_x/I_y, I_{max}/I_{min}) and quantify cortical bone thickness topographic variation across the preserved shaft portions by means of a 2-3D Relative Cortical Thickness index. Whenever possible, we also provided details about the site-specific organization of the cancellous network and measured the same parameters in a comparative sample of twelve adult extant humans. For most features, our results indicate two main patterns: the first includes the specimens TM 1517g, SKX 10924 and SKX 34805, while the second endostructural morphotype sets apart the robust *Homo* aff. *erectus* Gombore IB specimen from Melka Kunture, which more closely resembles the condition displayed by our

* Corresponding author. Computer-assisted Palaeoanthropology Team, UMR 5288 CNRS–Université Paul-Sabatier, Toulouse, France.
E-mail address: marine.cazenave4@gmail.com (M. Cazenave).

http://dx.doi.org/10.1016/j.crpv.2017.06.002

comparative human sample. Notably, marked differences in the amount and pattern of proximodistal cortical bone distribution have been detected between Gombore IB and SKX 34805 from Swartkrans. Given its discordant outer and inner signatures, we conclude that the taxonomic status of SKX 34805 deserves further investigations.

Mots clés :
Humérus distal
Structure interne
Topographie de l'os cortical
Paranthropus
Homo

RÉSUMÉ

Malgré leur abondance relative dans le registre fossile, l'attribution taxinomique d'huméri distaux isolés d'hominines a souvent été sujet d'incertitudes et de désaccords. Sur la base de variations de la morphologie externe de sections transversales d'un ensemble de spécimens du Plio-Pléistocène d'Afrique orientale et méridionale, quatre morphotypes, représentant respectivement *P. boisei*, *P. robustus*, premier *Homo* non-*erectus* et *H. erectus*, ont été récemment identifiés (Lague, 2015). Cependant, l'existence de possibles différences entre *Paranthropus* et *Homo* dans l'organisation de la structure interne de ce site squelettique reste inconnue. Nous avons utilisé des techniques d'imagerie non invasives pour caractériser l'organisation endostructurale de cinq huméri distaux d'Afrique du Sud (TM 1517g, SK 24600, SKX 10924 et SKX 34805) et d'Éthiopie (Gombore IB), qui ont été variablement attribués, soit à *Paranthropus*, soit à *Homo*. Même si les spécimens étudiés révèlent des variations dans leur préservation dues à leur histoire taphonomique et diagénétique, à l'exception de SK 24600 provenant de Swartkrans, nous avons pu analyser comparativement des paramètres de géométrie de section au niveau de la coupe transversale la plus distale de la diaphyse (%CA, I_x/I_y, I_{max}/I_{min}) et quantifier les variations topographiques d'épaisseur du tissu cortical le long de la portion diaphysaire préservée à l'aide d'indices 2–3D. Nous avons aussi apporté des précisions sur l'organisation site-spécifique du réseau trabéculaire et mesuré les mêmes variables dans un échantillon comparatif composé de douze humains actuels adultes. Pour la plupart des caractères, nos résultats indiquent deux patrons principaux : le premier réunit les spécimens TM 1517g, SKX 10924 et SKX 34805, tandis que le second morphotype endostructural distingue le spécimen robuste *Homo* aff. *erectus* de Melka Kunture, Gombore IB, qui se rapproche de la condition de l'échantillon comparatif humain. En particulier, des différences marquées dans la quantité et le patron de distribution proximo-distale de l'os cortical ont été détectées entre Gombore IB et SKX 34805 de Swartkrans. Compte tenu d'un certain dégrée d'hétérogénéité entre la morphologie externe et la signature morphostructurale interne, nous concluons que le statut taxonomique de SKX 34805 mérite d'autres analyses.

1. Introduction

The rarity in the hominin fossil record of unambiguously associated craniodental and postcranial remains usually complicates the task of identifying isolated fragmentary elements from the axial and the appendicular skeleton (e.g., Domínguez-Rodrigo et al., 2013; Hlusko et al., 2015; Lague, 2015). This is especially true for the hominin-bearing southern African cave sites, where variably preserved remains of *Australopithecus*, *Paranthropus* and *Homo* have been sometimes discovered commingled and where taxonomic diversity is revealing wider than previously assumed (Berger et al., 2010, 2015).

An interesting case is represented by the long-term debate about the allocation to *Paranthropus* (or australopith *s.l.*, following some authors) or *Homo* of isolated remains of the distal humerus remains (e.g., Bacon, 2000; Churchill et al., 2013; Di Vincenzo et al., 2015; Lague, 2014, 2015; Lague and Jungers, 1996; Patterson and Howells, 1967; Senut, 1981a; Susman, 1989; Susman et al., 2001). While potentially well suited for assessing postcranial variation because of their abundance in the record and the biomechanical specificities of the hominin elbow joint, Plio-Pleistocene specimens from both eastern and southern Africa have nonetheless been the matter of frequent controversial attributions (rev. in Domínguez-Rodrigo et al., 2013; Lague, 2015).

Compared to humans, the surface morphology of the distal humerus of *Paranthropus* is reported to show a mediolaterally broader and anteroposteriorly flatter distal shaft cross section (but see Domínguez-Rodrigo et al., 2013 for OH 80–10) with a more medially elongated articular surface, a more prominent coronoid fossa and a position of the lateral epicondyle above the upper edge of the capitulum (rev. in Di Vincenzo et al., 2015). Conversely, a poorly distinct coronoid area, a more distal positioning of the lateral epicondyle relative to the capitulum, a thick and medially oriented medial epicondyle (epitrochlea), a more vertically developed (thus, sub-rounded) and anteriorly projecting capitulum, and a proportionally anteroposteriorly expanded contour of the distal shaft are more typical human features (e.g., Di Vincenzo et al., 2015; Domínguez-Rodrigo et al., 2013; Lague, 2014; Susman, 1989; Susman et al., 2001). Also, the presence of a distally flaring sharp

supracondylar crest, also present in apes (Lague, 2015), seems more common in later *Homo* than in *Paranthropus*, even if rather variable in its occurrence and degree of development within the same fossil sample (Lague, 2015). For the inner structural organization, a thicker cortical bone and the diffuse presence of trabeculae nearly obstructing the most distal portion of the medullary cavity have also been reported as common features in *Paranthropus* (Domínguez-Rodrigo et al., 2013; Susman et al., 2001).

Besides the interspecific differences, a certain degree of intraspecific variation in fossil hominin distal humeral shaft morphology has been reported (Domínguez-Rodrigo et al., 2013; Feuerriegel et al., 2016; Lague, 2014, 2015). Notable inter-population variation in humeral shape (more elliptical vs. more circular diaphyses) has been measured also in *Pan troglodytes*, and could partly be attributed to differences in activity levels (Carlson et al., 2008). With this respect, the role of the still poorly determined extent of intraspecific sexual dimorphism is commonly evoked (e.g., Domínguez-Rodrigo et al., 2013; Feuerriegel et al., 2016; Lague, 2014).

Given the well-documented ability of long bones to adjust structurally to their loading environment, i.e. of recording relevant biomechanical information during life, but also of preserving the signature of their genetic-related evolutionary adaptive *bauplan* (Carlson and Marchi, 2014; Carlson et al., 2008; Currey, 2002; Gosman et al., 2011; Kivell, 2016; Lieberman et al., 2004; Lovejoy et al., 1999; Middleton et al., 2008; Nadell and Shaw, 2015; Pearson and Lieberman, 2004; Ruff et al., 2006; Ryan and Shaw, 2013; Smith-Adaline et al., 2004; Volkman et al., 2003; Wallace et al., 2010, 2012), an increasing number of studies use high resolution imaging techniques to reveal the inner structure of the fossil hominin humerus (e.g., Kappelman et al., 2016; Ruff et al., 2016; Ryan and Sukhdeo, 2016).

In this study, we noninvasively explored and quantitatively characterized the still unreported endostructural organization of five early Pleistocene distal humeri from South Africa (TM 1517g, SK 24600, SKX 10924, SKX 34805) and Ethiopia (Gombore IB), which have been variably attributed to *Paranthropus* or *Homo* (rev. in Lague, 2015). By assuming that the inner features at this skeletal site – notably, cross-sectional geometric properties and cortical bone topography – are taxon-specific to an extent comparable to the outer morphological signature, which has been commonly considered in their taxonomic assessment, we compare for their coherence the two signals.

Specifically, we expect that the inner structural arrangement of the South African fossils attributed to *Homo* (notably, SKX 34805 and, likely, SK 24600; Lague, 2015) will more closely resembles that of the *Homo* aff. *erectus* distal humerus Gombore IB than the endostructural signature of those specimens commonly attributed to *Paranthropus* (i.e. TM 1517g and SKX 10924).

2. Materials and methods

2.1. Materials

Information on the five fossil hominin distal humeri considered in the present study (TM 1517g, SK 24600, SKX 10924, SKX 34805, and MK 76 GOM IB 7594), all undistorted and sampling nearly or full adult individuals, is summarized in Table 1. They are permanently stored at the Ditsong National Museum of Natural History, Pretoria (TM 1517g and SK 24600), the Evolutionary Studies Institute at the University of the Witwatersrand, Johannesburg (SKX 10924 and SKX 34805), and at the National Museum of Ethiopia, Addis Ababa (MK 76 GOM IB 7594).

Originally reported by Broom (1938a) and detailed by Straus (1948), TM 1517g is an incomplete but well-preserved right distal humerus from the South African site of Kromdraai B (KB), part of the type specimen of *Paranthropus robustus* (Broom, 1938b; Broom and Schepers, 1946), which represents a dentally late adolescent individual (Braga et al., 2016a). More recent field work and material revision (rev. in Braga and Thackeray, 2016) suggest that, while commonly referred to KB Member 3 (e.g., Herries et al., 2009; Skinner et al., 2013; Thackeray et al., 2001; Vrba, 1981), TM 1517g and the purportedly associated remains are possibly from Member 5 (Braga et al., 2016a, b; but see Bruxelles et al., 2016: 42).

SK 24600 is a 2.3-1.6 Ma old distal part of an intact left humerus from Swartkrans Member 1, South Africa, preserving approximately the same anatomical region as the specimen SKX 10924. In its original description, Susman and co-workers (Susman et al., 2001: 617) stated that "(t)hese differences, and comparisons with TM 1517 and KNM-ER 271 as well as with modern humans, chimpanzees and bonobos, suggest that SK 24600 samples *Paranthropus*." However, based on the results of a recent geometric morphometric (GM) comparative analysis, this specimen has been allocated to early *Homo* (Lague, 2015).

SKX 10924, chronologically the most recent among the fossil specimens examined here ($\leq$ 1.0 Ma), is an intact distal left humeral end from Swartkrans Member 3, which has been described by Susman et al. (2001). Based on comparisons with SKX 34805 (Susman, 1989), and notably because of its "rounded" cross section, this specimen was originally allocated to *Homo* and was suggested to represent a small body-sized, probably female individual (Susman et al., 2001: 616). However, while it has been noted that SKX 10924 is considerably smaller than the TM 1517 g *P. robustus* specimen from Kromdraai (Susman et al., 2001), McHenry and Brown (2008) still included it among the remains more likely sampling *P. robustus* (see also Grine, 2005a). Even if still listed among the human remains by Dusseldorp et al. (2013: Suppl. Mat.; see Herries et al., 2009), an attribution of SKX 10924 to *Paranthropus* has been recently supported also by GM analyses (Lague, 2014, 2015).

SKX 34805 is a 2.3–1.6 Ma old distal part of a right humerus from Swartkrans Member 1 lacking a portion of each condyle, as well as the trochlea and the capitulum (Susman, 1989). In its original description, Susman stated that "(t)his specimen is a reasonably good match for TM 1517 in both size and shape, and on this basis it most likely belongs to *Paranthropus*" (Susman, 1989: 462). However, based on its cross-sectional shape and comparisons with the expanded record at Swartkrans, this specimen has since been allocated to *Homo* (Lague, 2015; Susman et al., 2001;

Table 1
The fossil specimens used in the present study.
Tableau 1
Les spécimens fossiles inclus dans cette étude.

Specimen	Site	Age (Ma)	Taxonomic attribution[a]	References
TM 1517g	Kromdraai (possibly Member 5[b]), South Africa	~2.0?[c]	*Paranthropus robustus*	Braga et al., 2016a, b; Broom, 1938b; Broom and Schepers, 1946; Bruxelles et al., 2016; Churchill et al., 2013; Di Vincenzo et al., 2015; Lague, 2014, 2015; Lague and Jungers, 1996; McHenry and Brown, 2008; Ryan and Sukhdeo, 2016; Senut, 1981a; Skinner et al., 2013; Straus, 1948; Susman, 1989; Susman et al., 2001; Thackeray et al., 2001
SK 24600	Swartkrans, Member 1, South Africa	2.3–1.6[c]	*Paranthropus robustus*	Churchill et al., 2013; Lague and Jungers, 1996; McHenry and Brown, 2008; Ryan and Sukhdeo, 2016; Susman et al., 2001
			early *Homo*	Lague, 2014, 2015
SKX 10924	Swartkrans, Member 3, South Africa	≤ 1.0[d]	*Paranthropus robustus*	Churchill et al., 2013; Lague, 2014, 2015; McHenry and Brown, 2008; Ryan and Sukhdeo, 2016
			Homo sp.	Susman et al., 2001; Dusseldorp et al., 2013 (in Suppl. Mat.)
SKX 34805	Swartkrans, Member 1, South Africa	2.3–1.6[c]	*Paranthropus robustus*	Susman, 1989
			early *Homo*/ *Homo* aff. *erectus*	Dusseldorp et al., 2013 (in Suppl. Mat.); Lague, 2015; Susman et al., 2001
MK 76 GOM IB 7594 (GOM IB)	Gombore I, Melka Kunture, Ethiopia	1.6–1.5[e]	*Homo* aff. *erectus*	Carretero et al., 2009; Chavaillon et al., 1977; Churchill et al., 2013; Di Vincenzo et al., 2015; Puymerail et al., 2014; Ryan and Sukhdeo, 2016; Senut, 1979, 1981a, b

[a] In some papers cited in this study, the taxon *Paranthropus* is subsumed within *Australopithecus*.
[b] Braga et al., 2016a, b; Bruxelles et al., 2016.
[c] Balter et al., 2008; Curnoe et al., 2001; Gibbon et al., 2014; Pickering et al., 2011; Vrba, 1981, 1985.
[d] Balter et al., 2008; Brain, 1993; Gibbon et al., 2014; Herries et al., 2009.
[e] Morgan, 2014 (pers. comm. to R.M.); Morgan et al., 2012; Tamrat et al., 2014.

see also Dusseldorp et al., 2013), more specifically, to *H.* aff. *erectus* (Lague, 2015).

Finally, Gombore IB (MK 76 GOM IB 7594, hereafter GOM IB) is a finely preserved distal third of a left humerus from a *Homo* aff. *erectus* robust individual. It was discovered in 1976 in the Oldowan tool-bearing level of Gombore I, one of the early to middle Pleistocene localities forming the Melka Kunture archaeological and paleontological site complex along the Upper Awash Valley, on the Ethiopian highlands (Chavaillon and Piperno, 2004; Gallotti and Mussi, 2015). Originally reported by Chavaillon and co-workers (1977) and by Senut (1979; see also Senut, 1981a, b), GOM IB has been more recently investigated by Puymerail et al. (2014) and by Di Vincenzo et al. (2015). A refinement of the chronologies at Melka Kunture (Morgan et al., 2012; Tamrat et al., 2014) indicates that GOM IB is 1.6-1.5 Ma old (Morgan, 2014: pers. comm. to R.M.), thus just slightly younger than the juvenile human partial mandible from the nearby site of Garba IV (Zanolli et al., 2016).

For this study, we used an extant human (EH) sample consisting of twelve adult humeri selected from the Pretoria Bone Collection stored in the Department of Anatomy at the University of Pretoria, South Africa (L'Abbé et al., 2005). The sample includes two male and four female individuals of African origin aged 23–29 years, and four male and two female European-derived individuals aged 41–58 years. All specimens used in this study lack any macroscopic evidence of outer or inner alteration or pathological change.

2.2. Methods

The South African fossil specimens TM 1517g, SK 24600, SKX 10924 and SKX 34805 and the twelve humeri forming the extant human comparative sample (EH) have been scanned between 2015 and 2016 at the micro-focus X-ray tomography facility (MIXRAD) of the South African Nuclear Energy Corporation (Necsa), Pelindaba, at resolutions ranging from 33 μm (fossil specimens) to 90 μm isotropic voxel size (EH sample) using a Nikon XTH 225 ST equipment (Hoffman and de Beer, 2012). Acquisition parameters for each of the four fossil specimens were as follow: 125 kV and 110 mA current, with a frame rate of 4 frames per second and an angular increment of 1000/360° resulting in an exposure time of 0.25 s/projection; 0.10 mm of aluminium was used to "pre-filter" low-energy X-rays. The specimen GOM IB from Melka Kunture was scanned in 2013 at the Wudassie Diagnostic Centre of Addis Ababa, Ethiopia, using a Philips Brilliance16 medical CT equipment according to the following parameters: 140 kV voltage, 100 mA current, 1.76 s exposition time per projection, slice thickness of 0.6 mm, reconstruction increment of 0.3 mm (see Zanolli et al., 2016). The final volume was reconstructed with a voxel size of 147 × 147 × 300 μm. In all cases, special care was taken in orienting each specimen

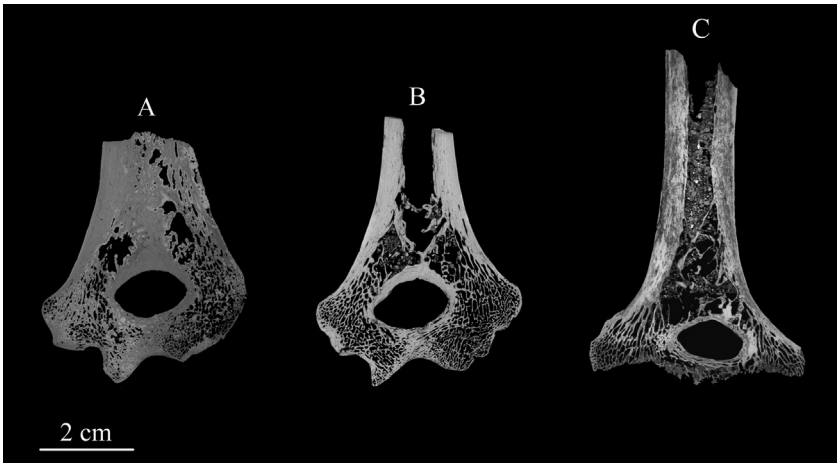

Fig. 1. µCT-based coronal slice of SK 24600 (A), SKX 10924 (B) and SKX 34805 (C), all from the site of Swartkrans, South Africa. Note their variable degree of inner preservation and the sedimentary infill and degree of mineralisation in SK 24600.
Fig. 1. Coupe coronale extraite des données µCT de SKX 24600 (A), SKX 10924 (B) et SKX 34805 (C) provenant du site de Swartkrans, Afrique du Sud. Noter le degré variable de conservation de la structure interne et du remplissage sédimentaire, ainsi que le degré de minéralisation pour SK 24600.

in a standardized way during acquisition (see comments in Wilson and Humphrey, 2015). Each diaphyseal axis was assessed as perpendicular to the coronal axis through the most medial and the most lateral points of the two epicondyles (the biepicondylar line). Coherence in orientation was then checked on the virtually reconstructed 3D models and, if needed, manually corrected by using Avizo© v.8.1 (Visualization Sciences Group Inc.).

In order to virtually isolate the cortical shell from the matrix variably filling the fossil specimens, to image their preserved inner morphology, and to quantify the cortical volume, a semi-automatic threshold-based segmentation with manual corrections was carried out (Spoor et al., 1993; see also Meyer and Beucher, 1990; Roerdink and Meijster, 2000) by using Avizo© v.8.1 (Visualization Sciences Group Inc.). In principle, while time-consuming because of frequent manual interventions, the segmentation process of SKX 10924, SKX 34805, and GOM IB did not present technical problems. As their endosteal contours were generally distinct at most shaft levels, the results of repeated performances independently run by two (in some cases, three) trained observers were consistent. However, because of its pervasive matrix infill, in SK 24600 the endosteal border was nearly invariably indistinguishable (Fig. 1), which presented challenges in using this specimen for the specific purposes of the present study (see infra section 3.1.). Also, some technical problems were encountered during the segmentation of TM 1517g, notably in precisely defining the endosteal contour along its lateral aspect.

Following the protocol established by Susman et al. (2001), and also adopted by Lague (2015), on each specimen we extracted a cross-sectional slice *a* at the humeral distal end, perpendicular to the major diaphyseal axis, approximately at the root of the medial crest slope, proximally to the biepicondylar line (Fig. 2). For the comparative assessment of proximodistal trends of thickness variation in cortex distribution across the shaft and for their 3D imaging, in all specimens except for the least preserved TM 1517g, we established an additional cross-sectional slice *b*, parallel to *a*, defined as the most proximal diaphyseal section (i.e. the most distant from *a*) preserving a complete periosteal and endosteal contour (Fig. 2). In our fossil sample, the maximal *a*–*b* distance is found in GOM IB, which also preserves the absolute longest shaft portion (biomechanical length in GOM IB has been estimated at ca. 339 mm, and its preserved shaft portion comprised between ca. 12% distally to ca. 30% proximally; Puymerail et al., 2014). However, to allow comparisons, we considered as reference the *a*–*b* distance found in SKX 34805 (36.4 mm), i.e. that of the second best preserved shaft following GOM IB. In SKX 10924, this distance measures 15.6 mm. However, it should be taken into account here that, because of the different preservation conditions among the investigated specimens and in the absence of percentages of their overall diaphyseal length, the shaft portions *a*–*b* do not necessarily fully coincide. Nonetheless, we estimate such differences as minimal and of negligible biomechanical relevance.

By using ImageJ and a custom macro (MomentMacro, available at: www.hopkinsmedicine.org/fae/mmacro.htm), at virtual slice level *a* we assessed the following cross-sectional geometric parameters (CSG) reflecting bone shaft morphological and rigidity characteristics: percent of cortical area (%CA), an estimate of resistance to compressive and tensile axial loading; the ratios second (I_x/I_y) and principal (I_{max}/I_{min}) moments of area, with the former ratio being a better estimate of rigidity about AP and ML anatomical planes and the latter shape ratio being the best reflection of true cross-sectional shape (Carlson, 2014; Ruff, 2002, 2008; Trinkaus and Ruff, 2012).

Cortical thickness varies topographically within each section and at various cross-sectional levels (for a schematic representation, see fig. 14.6 in White et al.,

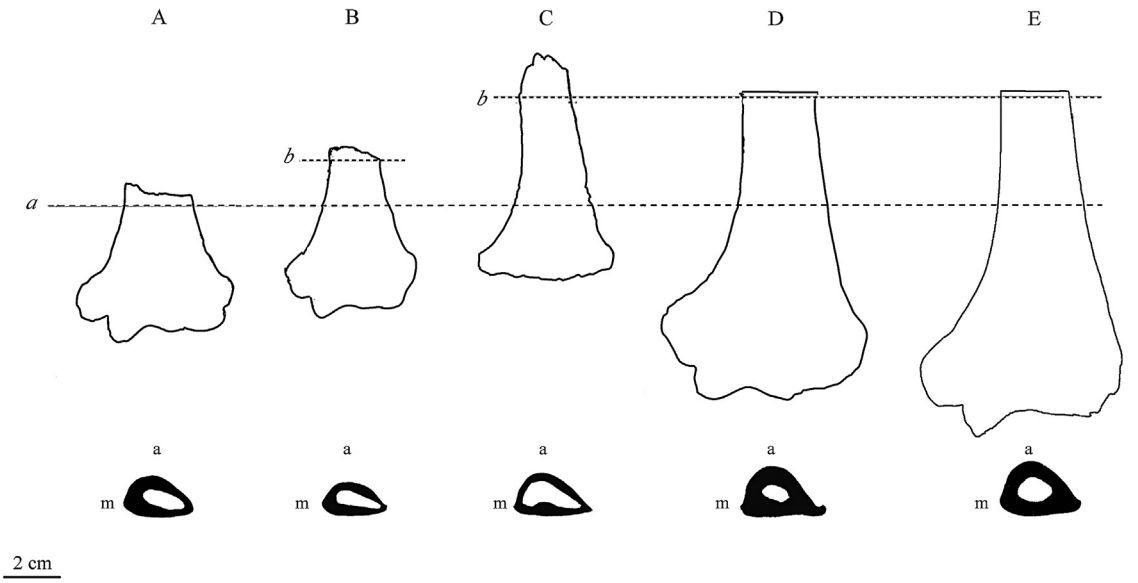

Fig. 2. Anterior view outline (upper row) and sketch of the cross section at level *a* (lower row) of the South African distal humeri TM 1517g (A), SKX 10924 (B) and SKX 34805 (C), of the Ethiopian specimen GOM IB (D), and of an extant human (EH) humerus. TM 1517g (A) and SKX 34805 (C) have been mirrored to be left. See the text (*2.2. Methods*) for details about the cross-sectional level *b*. The *a*–*b* distance measures 15.6 mm in SKX 10924 (B) and 36.4 mm in the remaining specimens. a: anterior; m: medial.

Fig. 2. Contours en vue antérieure (en haut) et schémas de la section extraite au niveau *a* (en bas) des huméri distaux sud-africains TM 1517g (A), SKX 10924 (B) et SKX 34805 (C), du spécimen éthiopien GOM IB (D) et d'un humérus humain actuel (EH). Un effet miroir a été appliqué pour TM 1517g (A) et SKX 34805 (C) afin d'obtenir des huméri gauches. Voir le texte (*2.2. Methods*) pour les détails à propos du niveau *b* de la coupe. La distance *a*–*b* est de 15,6 mm chez SKX 10924 (B) et de 36,4 mm pour les autres spécimens. A : antérieur ; m : médial.

2012). Accordingly, for the *a*–*b* shaft portion, we calculated a scale-free bi- (2D) and three-dimensional (3D) Relative Cortical Thickness (RCT) similarly to the analytical protocols used to allow a reliable comparative assessment of tooth enamel thickness variation in analyses using differently sized and shaped teeth (e.g., Grine, 2005b; Kono, 2004; Macchiarelli et al., 2006; Martin, 1985; Olejniczak et al., 2008). The 2D RCT is the average cortical thickness (2D ACT) multiplied by 100 and divided by the square root of the medullary cavity area (ma, in mm^2) (2D RCT = 2D ACT $\times$ $100/ma^{1/2}$), where 2D ACT is the ratio between cortical area (CA, in mm^2) and the endosteal contour length (ecl, in mm) (2D ACT = CA/ect, in mm); the 3D RCT is the average cortical thickness (3D ACT) multiplied by 100 and divided by the cube root of the medullary cavity volume (mv, in mm^3) (3D RCT = 3D ACT $\times$ $100/mv^{1/3}$), where 3D ACT is the ratio between cortical volume (cv, in mm^3) and the area of the endosteal surface (aes, in mm^2) (3D ACT = cv/aes, in mm) (for the Relative Enamel Thickness, see technical details in Olejniczak et al., 2008). As the Relative Enamel Thickness (RET) provides a scale-free measure of the enamel tissue with respect to the dentine, which is especially appropriate for interspecies comparisons (Martin, 1985), the RCT finely assesses cortical bone thickness across a shaft portion with respect to the space occupied by the medullary cavity (and by the struts as well). This synthetic descriptor of bone thickness variation adds useful complementary information, notably at volumetric scale, to the traditional geometric parameters punctually assessed at cross-sectional level and allows a finer interpretation of the long bone morphometric maps (Bondioli et al., 2010).

Intra- and inter-observer tests for measurement accuracy showed differences less than 4%.

For each anatomical projection (i.e. anterior, posterior, medial and lateral views), cortical thickness topographic distribution between *a* and *b* has been virtually rendered in all fossil specimens except TM 1517g using a chromatic scale increasing from dark blue (thin) to red (thick) (Bayle et al., 2011; Bondioli et al., 2010; Mazurier et al., 2010; Puymerail, 2011, 2013; Puymerail et al., 2012; Volpato et al., 2011).

Given the variable degree of endostructural preservation of the South African specimens (see infra 3.1) and the modest resolution of the CT record available for the distal humerus from Melka Kunture, in this study we did not assess the textural properties of the cancellous network, but uniquely provided, whenever possible, information on the presence/absence and type of trabecular structures.

3. Results

3.1. Inner preservation

The fossil specimens considered in this study show a variable degree of inner preservation and quality of the structural signal, ranging from rather good to very poor. As previously noted for the cancellous network of some South African australopith iliac blades (Macchiarelli et al., 1999), the inner structural conservation is unrelated to the outer preservation conditions, and here it extensively varies between specimens from the same site (or even from the same Member, as is the case of SK 24600 and SKX 34805

from Swartkrans) and between areas within the same specimen (Fig. 1).

In TM 1517g, the cancellous struts at the very distal shaft portion and epiphyseal end are arranged in a distinctly appreciable network, even if the trabeculae boundaries are locally masked by a matrix infill. Conversely, in SK 24600 the entire cavity is filled by highly cemented permeating matrix, which nearly invariably inhibits the identification of the cortex-cavity boundary because of their close material contrast (Fig. 1A). Additionally, in this specimen, the preserved cancellous network has a low contrast between the bone and the matrix due to similar densities of the two entities which cannot be satisfactorily overcome by digital image processing of the currently available record. Accordingly, SK 24600 has been a posteriori excluded from all quantitative analyses performed in this study.

Among the investigated fossil specimens, SKX 10924 revealed the most finely preserved inner structure (Fig. 1B). However, while its cancellous network is virtually intact, the identification of the bone-cavity boundary was locally disturbed by the presence of a relatively thin matrix layer, which obliged us to carry out a number of manual corrections to the semi-automatic threshold-based segmentation. The last specimen from Swartkrans included in this study, SKX 34805 also showed a sufficiently well-preserved cancellous network but, compared to SKX 10924, it is variably filled with a consolidated matrix whose density was, anyhow, distinct enough from that of the cortex (Fig. 1C).

Finally, despite its medullary cavity being filled with matrix, the preservation conditions of the Ethiopian specimen GOM IB, where only the cancellous network at its distal end showed a low bone-matrix contrast, permitted an unambiguous segmentation of its cortex.

3.2. *Structural arrangement and cortical thickness variation*

At cross-sectional level *a*, a mediolaterally broad and proportionally anteroposteriorly flattened elliptically-shaped medullary cavity is noticeable in TM 1517g (M-L/A-P diameter ratio: 1.7), SKX 10924 (ratio: 1.9) and SKX 34805 (ratio: 1.8) (Fig. 2A-C), while GOM IB (Fig. 2D) shows a sub-ovoid outline (i.e. slightly more expanded anteroposteriorly compared to an elliptically-shaped outline; M-L/A-P diameter ratio: 1.6), more closely approaching the extant human condition represented in our comparative sample (Fig. 2E), where it varies from sub-ovoid to sub-rounded (mean ratio: 1.5 ± 0.15).

At this distal shaft level, notably towards the lateral aspect, a variable number of relatively thick trabecular struts, occasionally crossing the cavity at various points, are present in all fossil specimens, which is commonly not the case in extant humans (besides our reference sample, see also Diederichs et al., 2009). Struts are especially numerous and thick in SKX 10924 and, to a slightly minor extent,

Table 2
Cross-sectional geometric properties (CSG) of the distal humeral diaphysis assessed at section *a* (see Fig. 2) in four fossil specimens and in the extant human reference sample (EH). s.d.: standard deviation.
Tableau 2
Paramètres de géométrie de section (CSG) mesurés à la section *a* (voir Fig. 2) pour quatre spécimens fossiles et pour notre échantillon humain actuel de référence (EH). s.d. : déviation standard.

Specimen/ sample	%CA	I_x/I_y	I_{max}/I_{min}
TM 1517 g	75.7	0.43	2.43
SKX 10924	72.4	0.35	2.94
SKX 34805	62.9	0.40	2.51
GOM IB	89.7	0.51	2.33
extant humans (EH)	63.2	0.92	1.94
(s.d.)	(11.6)	(0.61)	(0.31)

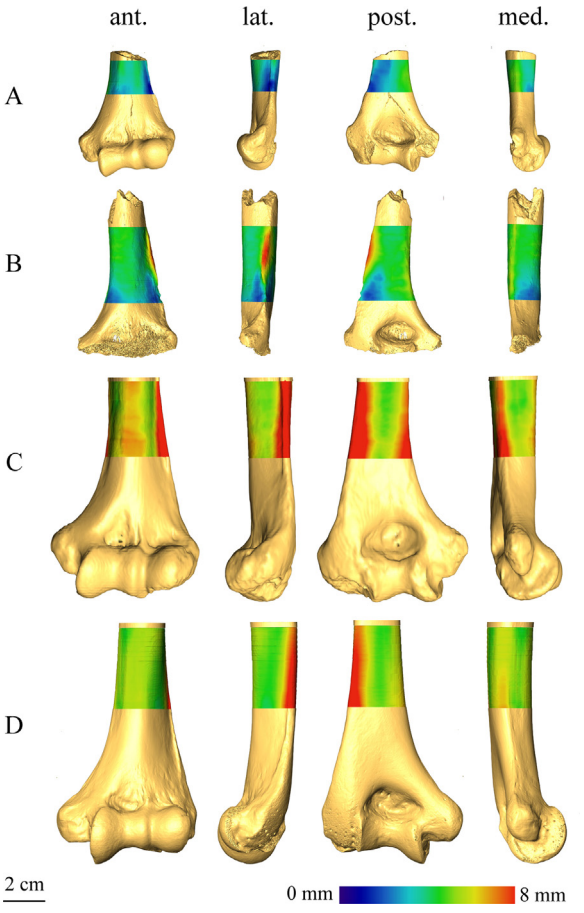

Fig. 3. (μ)CT-based maps of cortical bone thickness topographic distribution in anterior (ant.), posterior (post.), medial (med.), and lateral (lat.) views assessed along the shaft portion *a*–*b* (see Fig. 2) in the South African distal humeri SKX 10924 (A) and SKX 34805 (B), in the Ethiopian specimen GOM IB (C), and in an extant human (EH) humerus (D). SKX 34805 has been mirrored to be left. Thickness rendered by a chromatic scale increasing from dark blue (0 mm) to red (8 mm) for the *a*–*b* shaft portion (see Fig. 2).
Fig. 3. Reconstruction sur base microtomographique de la distribution topographique des variations d'épaisseur de l'os cortical dans la portion diaphysaire *a*–*b* (voir Fig. 2) des huméri distaux sud-africains SKX 10924 (A) et SKX 34805 (B), du spécimen éthiopien GOM IB (C) et d'un humérus humain actuel (EH, D) en vues antérieure (ant.), postérieure (post.), médiale (med.) et latérale (lat.). Un effet miroir a été appliqué pour SKX 34805 (B) afin d'obtenir un humérus gauche. Les épaisseurs sont représentées selon une échelle chromatique variant du bleu foncé (0 mm) au rouge (8 mm) pour la portion de diaphyse *a*–*b* (voir Fig. 2).

in SKX 34805, where they can locally form some plate-like structures (Gibson, 1985; Stauber and Müller, 2006), including towards the medial portion. Because of the permeating infill, the cancellous pattern is however difficult to discern in TM 1517g, but here the struts are uniquely confined to the lateral quadrant, which is not the case in the two fossils from Swartkrans. Given its mediolaterally narrower cavity, in GOM IB the struts are less numerous, even if not necessarily thinner than seen in SKX 10924 and SKX 34805.

The values of the CSG properties measured at section *a* are shown in Table 2. For the percent of cortical area (%CA), the highest value is shown by the distal humerus from Melka Kunture (89.7), which is over 2 standard deviations (s.d.) beyond the average expressed by our comparative extant human sample (63.2 ± 11.6). Among the South African specimens, TM 1517g shows the highest value (75.7), while the two distal humeri from Swartkrans fall within 1 s.d. (SKX 10924: 72.4), or just near the mean of the reference sample (SKX 34805: 62.9). As a whole, the pattern for %CA is: GOM IB » TM 1517g > SKX 10924 > extant humans ≈ SKX 34805.

Variation for the ratio of anteroposterior vs. mediolateral second moments of area (I_x/I_y) is modest among the South African fossils (range: 0.35 in SKX 10924 to 0.43 in TM 1517g), whose values are exceeded by both GOM IB (0.51) and, to a greater extent, by the modern reference sample (0.92 ± 0.61). Because of the mediolateral expansion at such a distal diaphyseal level observed in all specimens (i.e. the maximum rigidity is in the mediolateral direction), this pattern is almost systematically reversed for the maximum vs. minimum second moments of area (I_{max}/I_{min}), where the results of all fossils (range: 2.33 in GOM IB to 2.94 in SKX 10924) are from 2 s.d. (GOM IB, TM 1517g, SKX 34805) to 4 s.d. (SKX 10924) beyond the average value of the comparative human sample (1.94 ± 0.31).

According to four anatomical views, the morphometric maps of cortical bone thickness topographic variation across the shaft portion *a*–*b* in SKX 10924, SKX 34805, GOM IB, and in an extant human (EH) representative selected within our comparative sample because of its average cortical distribution (3D RCT values), are shown in Fig. 3. As previously specified, such virtual rendering was not technically possible for TM 1517g because of its too limited preserved portion.

While the limited preserved shaft portion of SKX 10924 precludes a detailed 1:1 comparison, the 3D maps confirm a closer affinity in cortical bone distribution pattern between the two specimens from Swartkrans, on one hand, and GOM IB and the average extant human condition, on the other hand, the latter invariably displaying absolutely and relatively thicker bone at all sites. Specifically, the South African fossils share relatively thicker bone across most of the posteromedial and the proximal part of the anterior aspects (in SKX 34805 the thickest bone corresponds to its relatively developed lateral supracondylar crest), and a thinner area along the distolateral portion of the posterior surface, a region where GOM IB and all modern human humeri conversely show thicker bone. In GOM IB, and in the comparative human sample as well, thinner bone is found anteriorly, anterolaterally (when the lateral supracondylar crest is not considered) and along the mid-third of the posterior aspect. Similarly to SKX 34805 and to the extant human figures, cortical thickening in GOM IB indeed corresponds here to a well-developed and vertically extended lateral supracondylar crest forming the sharp pinched and slightly undulating border of the distal shaft (Puymerail et al., 2014). Thickened bone in the Ethiopian specimen is also found along its medial crest, which is more marked in this *Homo* aff. *erectus* humerus compared to the two South African fossils.

Although the absolute values cannot be systematically compared, to determine the extent of the differences among the morphometric maps, we calculated the trends of proximodistal variation of the 2D RCT (Table 3). The results confirm a trend of cortical bone thinning in SKX 34805 (−66%) and, by contrast, of thickening in GOM IB (+61%). The incomplete signal from SKX 10924 (shorter *a*–*b* portion) basically supports the evidence from the other more complete shaft from Swartkrans (−42%). Variation for this parameter expressed by our human reference sample (from −60% thinning to +17% thickening) is marked and requires additional investigation, but at present we have no data enough to even tentatively relate such variation to any

Table 3
Bi- (2D RCT) and three-dimensional cortical thickness (3D RCT) of the distal humeral diaphysis assessed within the portion comprised between section *b* and section *a* (see Fig. 2) in three fossil specimens and in the extant human reference sample (EH).
Tableau 3
Épaisseur corticale de la diaphyse humérale mesurée en 2–3D sur une portion de diaphyse comprise entre la section *b* et la section *a* (voir Fig. 2) dans trois spécimens fossiles et dans notre échantillon humain actuel de référence (EH).

Specimen/ sample	2D RCT total shaft portion *b* to *a* % change	2D RCT anterior shaft portion *b* to *a* % change	2D RCT posterior shaft portion *b* to *a* % change	3D RCT total shaft portion proximal[a] to distal[b] % change
SKX 10924[c]	−42%	−30%	−18%	–
SKX 34805	−66%	−39%	−23%	−41%
GOM IB	+61%	+90%	+81%	+51%
extant humans (EH) (range)	−60% to +17%	−33% to +12%	−38% to +26%	−37% to +9%

[a] Proximal is the shaft portion comprised between *b* and the *a*–*b* mid-distance level (see Fig. 2); it is equal in location to SKX 34805 and GOM IB, but not to SKX 10924.

[b] Distal is the shaft portion comprised between the *a*–*b* mid-distance level and *a* (see Fig. 2); it is equal in location to SKX 34805 and GOM IB, but not to SKX 10924.

[c] In SKX 10924, proximal level *b* approximately corresponds to the *a*–*b* mid-distance level of SKX 34805 and GOM IB (see Fig. 2).

individual information available in our files (e.g., sex, age at death). The comparisons for 3D RCTs assessed in SKX 34805 and GOM IB for their relative proximal and distal portions of the *a*–*b* shaft segment provide the same indication of proportional global volumetric thinning in the South African (−41%) and of thickening in the Ethiopian (+51%) specimen. When the more variably shaped medial and lateral aspects are excluded and the 2D RCT is separately calculated for the anterior and the posterior portions at the same cross sections *a* and *b*, we note that the trend (thinning or thickening) is always more marked on the anterior aspect across the distal diaphysis, including in SKX 10924 (Table 3). Finally, even though variation in recent humans requires some in-depth analyses performed on larger samples, the amount of changes in cortical bone thickness expressed in our reference sample by the 3D RCT is lower than the measured variation in the three fossil specimens (Table 3), and is compatible with the evidence from other CT-based studies of clinical interest (e.g., Diederichs et al., 2009).

4. Discussion and conclusions

In his extensive GM-based study of the outer cross-sectional shape variation of a representative sample of eastern and southern African fossil hominin distal humeri, Lague (2015) identified the following four morphotypes (group configuration): *P. boisei* (OH 80, KNM-ER 739, 1504, 6020, 1591), *P. robustus* (TM 1517, SKX 10924; recently, the specimen DNH 32 from Drimolen, South Africa, has been added to this list; Lague and Menter, 2017), non-*erectus* early *Homo* (OH 62, ER 3735, SK 24600, SKX 19495, SK 2598), and *H. erectus* (WT 15000, ER 1808, SKX 34805). Following his results, distal humeri representing non-*erectus* early *Homo* are distinguishable because of their degree of relative anteroposterior flattening, while the morphology of *H. erectus* is more similar to that typical of more recent humans. In this context, *Paranthropus s.l.* specimens from both eastern and southern Africa are characterized by a morphology intermediate with respect to the features that differentiate non-*erectus* early *Homo* and *H. erectus*. Accordingly, the lower diaphyses of *P. boisei* (not considered in our study) and of non-*erectus* early *Homo* are "unusually AP flattened (ML broad) among both fossil hominins and extant hominids, though non-*erectus Homo* humeri are most extreme in this regard and markedly different from the more modern human-like specimens attributed to *H. erectus*" (Lague, 2015: 27). Fresh evidence from the *A. sediba*'s ulna shows that, in aspects of its size and shape, the outer morphology of its elbow, which shows adaptations to suspensory and climbing behaviours (Rein et al., 2017), falls within the range of variation of eastern and southern australopiths, including some specimens commonly attributed to *P. robustus*, such as TM 1517 and SK 10294 (Churchill et al., 2013).

For most structural parameters of the distal humerus considered in the present study, we schematically observed two main patterns: the first globally grouping the South African fossils, and the second pattern setting apart the specimen from Melka Kunture (GOM IB), more closely resembling the extant human condition. In principle, even if the southern African fossil sample provides evidence of variation, a "dichotomy" is found here for: (i) the elliptical (proportionally flatter) vs. the ovoid (proportionally more expanded anteroposteriorly) outline of the medullary cavity at the distal diaphyseal cross section *a*, even if, in this case, the position of SKX 34805 can be seen as intermediate; (ii) thinner vs. thicker cortices (%CA) as measured at the same cross-sectional level; (iii) a cortical bone distribution pattern of proximodistal thinning vs. thickening across the portion*a*–*b* (as revealed by the 2–3D Relative Cortical Thickness parameters). With special reference to the latter aspect, the results unequivocally distinguish GOM IB from the organizational pattern shared by the two specimens from Swartkrans available to us for such kind of analysis (SKX 10924 and SKX 34805) (see also Fig. 3).

Conversely, even if a tendency for "dichotomy" between GOM IB and the South African fossils is traceable for the I_x/I_y and I_{max}/I_{min} ratios, the differences at the most distal diaphyseal level are modest and a dominant maximum rigidity in the mediolateral plane is shown by all specimens. However, it should be also noted that, compared to the global pattern shown by the extant reference sample, the three South African fossils share a looser connection between the two ratios, indicating a more oblique orientation component of their maximum rigidity, i.e. a less stereotyped mediolateral maximum rigidity at the humeroulnar joint. With this respect, among the fossils considered in the present study, GOM IB is again the specimen more closely approaching the modern pattern, and also that displaying the most developed, thickest and vertically extended lateral supracondylar crest, i.e. the origin of *M. brachioradialis*. Differences in the development of such muscle, which is responsible for both flexion of the forearm and pronation of a supine forearm, and supination of a prone forearm, are associated in extant humans with differences in flexion to extension movement patterns at the elbow (Rhodes and Knüsel, 2005). Specifically, in humans the *M. brachioradialis* primarily acts as elbow stabilizer during flexion tasks (Boland et al., 2008). Nonetheless, it is also true that a certain variation in the degree of expression of the supracondylar crest, as well as in the differences between maximum second moment of area, I_{max}, and second moment of area in the mediolateral plane, I_y (range: from 0 up to 48%) are present even within our limited reference sample.

Because of a number of reasons explained in the methodological section, in this study we did not systematically assess the textural properties of the cancellous network. It seems nonetheless interesting to note that, besides the ambiguous evidence from TM 1517g because of its low bone-matrix contrast, the two specimens from Swartkrans share the presence of more numerous and thick struts, locally resulting into a more closed network of plate-like structures from the accumulation of more material in the cell wall (Dalstra and Huiskes, 1995; Gibson, 1985; Stauber and Müller, 2006). At any comparable site, struts are invariably thicker in the fossil specimens than in the extant human humeri available to us, which is consistent with the process of skeletal gracilisation and trabecular bone density reduction occurred in recent humans (Chirchir et al., 2015, 2017; Ryan and Shaw, 2015). It is also noticeable that the medullary cavity of the OH

80-10 distal humerus fragment from the *P. boisei* partial skeleton of Olduvai Gorge, Tanzania, is filled by trabecular bone (Domínguez-Rodrigo et al., 2013). On the other hand, probably because of its narrower lumen resulting from a thicker cortex, GOM IB displays less numerous and less projecting struts, mostly confined to the very distal end.

When our results are considered in a taxonomic perspective, we note that the first pattern more coherently associates two likely *Paranthropus* representatives – TM 1517g from Kromdraai and SKX 10924 from Swartkrans – to a specimen more likely representing early *Homo* or *H.* aff. *erectus*– SKX 34805, again from Swartkrans. The second pattern unambiguously distinguishes the distal humerus of *Homo* aff. *erectus* from Melka Kunture from all other specimens, and frequently even clusters it near the extant human condition. Additionally, in this limited fossil assemblage, the closest endostructural signatures are clearly shown by SKX 10924 (even if incomplete) and SKX 34805. Relevant here also the evidence that the thickest cortex at any site across the distal shaft end is found in GOM IB (*Homo*) and not in any *Paranthropus*. Whenever SKX 34805 and GOM IB are grouped as conspecific (Lague, 2015), or at least congeneric (Susman et al., 2001), among the fossil specimens used in the present study they respectively show the absolutely lower (%CA: 62.9) and higher (%CA: 89.7) amount of cortical bone at section *a*.

Indeed, a relevant result here concerns the structural differences measured between SKX 34805 and GOM IB in their relative and absolute amount of cortical bone and distribution pattern shown across a comparable portion of 36.4 mm at the distal humeral shaft. This shows that even specimens with similar diaphyseal shape (Lague, 2015) may differ substantially in relative cortical thickness. Variations in the amount of cortical bone tissue (commonly measured by %CA) reflect site-specific differences in the bone's ability to buffer pure axial compression and tension, i.e. differential structural reinforcements of the diaphysis (Ruff, 2008; Trinkaus and Ruff, 2012). Accordingly, even if we cannot discard here the possible influence on the endostructural bony arrangement of sex-related (or even of age-related) differences, nor that of a different handedness (for a recent discussion on hand specialization in early *Homo*, see Frayer et al., 2016; for its impact on humeral cross-sectional shape variation and cortical bone thickness distribution, see Lague, 2015 and Volpato et al., 2012, respectively), we anyhow assume that the two distinct conditions ("patterns") revealed by the South African and the Ethiopian specimens, whatever their taxonomic status, are primarily functionally-related and have biomechanical significance in terms of distal humeral strength.

In this perspective, we conclude that the taxonomic status of SKX 34805, which apparently combines a relatively *Homo*-like outer shape (Lague, 2014, 2015) with a more *Paranthropus*-like inner structural organization of the distal humerus (present study), deserves further investigation.

Acknowledgments

The present study contributes to the thematic issue of the *Comptes rendus Palevol* "Hominin biomechanics, virtual anatomy and inner structural morphology: From head to toe. A tribute to Laurent Puymerail", promoted by C. Zanolli and R. Macchiarelli. Some of the authors were fortunate enough to interact with Laurent and to benefit from his unique research work, unfortunately unfinished, on the structural organization of the distal humerus from Melka Kunture.

This version greatly benefited from the competent critical comments provided by three reviewers. We also acknowledge the valuable suggestions provided by K.J. Carlson (Johannesburg and Los Angeles), M.R. Lague (Galloway) and D. Marchi (Pisa) during various phases of this study. For access to the fossil and comparative materials stored in South Africa, we are especially grateful to the curators of the Ditsong National Museum of Natural History, Pretoria, and the Pretoria Bone Collection at the Department of Anatomy of the University of Pretoria. Within the activities of the Italian Archaeological Mission at Melka Kunture and Balchit, authorization for performing the CT-scan record of MK 76 GOM IB 7594 was provided by the Authority for Research and Conservation of Cultural Heritage (ARCCH) of the Federal Democratic Republic of Ethiopia, and R.M. acknowledges for their kind support Y. Assefa, M. Mussi, Y.D. Tsegaye and Y. Yilma. For technical collaboration, scientific contribution and/or discussion, we are very grateful to L. Bam (Pelindaba), A. Beaudet (Johannesburg), J. Benoit (Johannesburg), B. Billings (Johannesburg), L. Bruxelles (Toulouse and Johannesburg), R.J. Clarke (Johannesburg), M. Domínguez-Rodrigo (Madrid), J. Dumoncel (Toulouse), D. Hailu (Addis Ababa), K. Jakata (Johannesburg), T. Jashashvili (Johannesburg), L. Kgasi (Pretoria), D. Marchi (Pisa), A. Mazurier (Poitiers), S. Potze (Pretoria), C. Ridel (Pretoria), D. Stratford (Johannesburg), C. Theye (Pretoria), V. Volpato (Fribourg), C. Zanolli (Toulouse), B. Zipfel (Johannesburg). We acknowledge the DST-NRF for the financial support (Grant # UID23456) to establish the MIXRAD micro-focus X-ray tomography facility at Necsa. M.C. is funded by the European Commission (EACEA), Erasmus Mundus programme, AESOP and AESOP+ consortia coordinated by J.B.

References

Bacon, A.-M., 2000. Principal components analysis of distal humeral shape in Pliocene to recent African hominids: the contribution of geometric morphometrics. Am. J. Phys. Anthropol. 111, 479–487.

Balter, V., Blichert-Toft, J., Braga, J., Telouk, P., Thackeray, F., Albarède, F., 2008. U-Pb dating of fossil enamel from the Swartkrans Pleistocene hominid site. South Africa. Earth Planet. Sci. Lett. 267, 236–246.

Bayle, P., Bondioli, L., Macchiarelli, R., Mazurier, A., Puymerail, L., Volpato, V., Zanolli, C., 2011. Three-dimensional imaging and quantitative characterization of human fossil remains. Examples from the NESPOS database. In: Macchiarelli, R., Weniger, G.-C. (Eds.), Pleistocene databases. acquisition, storing, sharing. Wissenschaftliche Schriften des Neanderthal Museums 4, Mettmann, pp. 29–46.

Berger, L.R., de Ruiter, D.J., Churchill, S.E., Schmid, P., Carlson, K.J., Dirks, P.H.G.M., Kibii, J.M., 2010. *Australopithecus sediba*: a new species of *Homo*-like australopith from South Africa. Science 328, 195–204.

Berger, L.R., Hawks, J., de Ruiter, D.J., Churchill, S.E., Schmid, P., Delezene, L.K., Kivell, T.L., Garvin, H.M., Williams, S.A., DeSilva, J.M., Skinner, M.M., Musiba, C.M., Cameron, N., Holliday, T.W., Harcourt-Smith, W., Ackermann, R.R., Bastir, M., Bogin, B., Bolter, D., Brophy, J., Cofran, Z.D., Congdon, K.A., Deane, A.S., Dembo, M., Drapeau, M., Elliott, M.C., Feuerriegel, E.M., Garcia-Martinez, D., Green, D.J., Gurtov, A., Irish, J.D., Kruger, A., Laird, M.F., Marchi, D., Meyer, M.R., Nalla, S., Negash, E.W., Orr, C.M., Radov_ci_c, D., Schroeder, L., Scott, J.E., Throckmorton, Z., Tocheri, M.W., VanSickle, C., Walker, C.S., Wei, P., Zipfel, B., 2015. *Homo*

naledi, a new species of the genus *Homo* from the Dinaledi Chamber, South Africa. eLife 4, 1–35.
Boland, M.R., Spigelman, T., Uhl, T.L., 2008. The function of brachioradialis. J. Hand Surg. 33, 1853–1859.
Bondioli, L., Bayle, P., Dean, C., Mazurier, A., Puymerail, L., Ruff, C., Stock, J.T., Volpato, V., Zanolli, C., Macchiarelli, R., 2010. Technical note. Morphometric maps of long bone shafts and dental roots for imaging topographic thickness variation. Am. J. Phys. Anthropol. 142, 328–334.
Braga, J., Thackeray, J.F., 2016. Kromdraai, a birthplace of *Paranthropus* in the cradle of humankind. Sun Press, Johannesburg.
Braga, J., Thackeray, J.F., Bruxelles, L., Dumoncel, J., Fourvel, J.-B., 2016b. Stretching the time span of hominin evolution at Kromdraai (Gauteng, South Africa): recent discoveries. C.R. Palevol 16, 58–70.
Braga, J., Dumoncel, J., Duployer, B., Tenailleau, C., de Beer, F., Thackeray, J.F., 2016a. The Kromdraai hominins revised with an updated portrayal of differences between *Australopithecus africanus* and *Paranthropus robustus*. In: Braga, J., Thackeray, J.F. (Eds.), Kromdraai, a birthplace of *Paranthropus* in the cradle of humankind. Sun Press, Johannesburg, pp. 49–68.
Brain, C.K., 1993. Swartkrans: a cave's chronicle of early man. Transvaal Museum, Pretoria.
Broom, R., 1938a. Further evidence on the structure of the South African Pleistocene anthropoids. Nature 142, 897–899.
Broom, R., 1938b. The Pleistocene anthropoid apes of South Africa. Nature 142, 377–379.
Broom, R., Schepers, G.W.H., 1946. The South African Fossil Ape-M: the Australopithecinae, n. 2. Transvaal Museum Memoir, Pretoria.
Bruxelles, L., Maire, R., Couzens, R., Thackeray, J.F., Braga, J., 2016. A revised stratigraphy of Kromdraai. In: Braga, J., Thackeray, J.F. (Eds.), Kromdraai, a birthplace of *Paranthropus* in the cradle of humankind. Sun Press, Johannesburg, pp. 31–46.
Carlson, K.J., 2014. Linearity in the real world: an experimental assessment of nonlinearity in terrestrial locomotion. In: Carlson, K.J., Marchi, D. (Eds.), Reconstructing mobility. Environmental, behavioral and morphological determinants. Springer, New York, pp. 253–271.
Carlson, K.J., Marchi, D., 2014. In: Carlson, K.J., Marchi, D. (Eds.), Reconstructing mobility. Environmental, behavioral and morphological determinants. Springer, New York.
Carlson, K.J., Sumner, D., Morbeck, M., Nishida, T., Yamanaka, A., Boesch, C., 2008. Role of nonbehavioral factors in adjusting long bone diaphyseal structure in free-ranging *Pan troglodytes*. Int. J. Primatol. 29, 1401–1420.
Carretero, J.M., Haile-Selassie, Y., Rodriguez, L., Arsuaga, J.L., 2009. A partial distal humerus from the Middle Pleistocene deposits at Bodo, Middle Awash, Ethiopia. Anthropol. Sci. 117, 19–31.
Chavaillon, J., Chavaillon, N., Coppens, Y., Senut, B., 1977. Présence d'hominidé dans le site oldowayen de Gomboré I à Melka Kunturé, Ethiopie. C.R. Acad. Sci. Paris, Ser. D 285, 961–963.
Chavaillon, J., Piperno, M. (Eds.), 2004. Studies on the Early Paleolithic site of Melka Kunture, Ethiopia. Instituto Italiano di Preistoria e Protostoria, Florence.
Chirchir, H., Kivell, T.L., Ruff, C.B., Hublin, J.-J., Carlson, K.J., Zipfel, B., Richmond, B.G., 2015. Recent origin of low trabecular bone density in modern humans. PNAS USA 112, 366–371.
Chirchir, H., Ruff, C.B., Junno, J.-A., Potts, R., 2017. Low trabecular bone density in recent sedentary modern humans. Am. J. Phys. Anthropol. (online version).
Churchill, S.E., Holliday, T.W., Carlson, K.J., Jashashvili, T., Macias, M.E., Mathews, S., Sparling, T.L., Schmid, P., de Ruiter, D.J., Berger, L.R., 2013. The upper limb of *Australopithecus sediba*. Science 340, 1233477–1233481.
Curnoe, D., Grün, R., Taylor, L., Thackeray, F., 2001. Direct ESR dating of a Pliocene hominin from Swartkrans. J. Hum. Evol. 40, 379–391.
Currey, J.D., 2002. Bones: structure and mechanics. Princeton University Press, Princeton.
Dalstra, M., Huiskes, R., 1995. Load transfer across the pelvic bone. J. Biomech. 28, 715–724.
Diederichs, G., Issever, A.-S., Greiner, S., Linke, B., Korner, J., 2009. Three-dimensional distribution of trabecular bone density and cortical thickness in the distal humerus. J. Should. Elb. Surg. 18, 399–407.
Di Vincenzo, F., Rodriguez, L., Carretero, J.M., Collina, C., Geraads, D., Piperno, M., Manzi, G., 2015. The massive fossil humerus from the Oldowan horizon of Gombore I, Melka Kunture (Ethiopia, > 1.39 Ma). Quat. Sci. Rev. 122, 207–221.
Domínguez-Rodrigo, M., Pickering, T.R., Baquedano, E., Mabulla, A., Mark, D.F., Musiba, C., Pérez-González, A., 2013. First partial skeleton of a 1.34-million-year-old *Paranthropus boisei* from Bed II, Olduvai Gorge, Tanzania. PLoS ONE 8, e80347.
Dusseldorp, G., Lombard, M., Wurz, S., 2013. Pleistocene *Homo* and the updated Stone Age sequence of South Africa. S. Afr. J. Sci. 109, 1–7.
Feuerriegel, E.M., Green, D.J., Walker, C.S., Schmid, P., Hawks, J., Berger, L.R., Churchill, S.E., 2017. The upper limb of *Homo naledi*. J. Hum. Evol. 104, 155–173.
Frayer, D.W., Clarke, R.J., Fiore, I., Blumenschine, R.J., Pérez-Pérez, A., Martinez, L.M., Estebaranz, F., Holloway, R., Bondioli, L., 2016. OH-65: the earliest evidence for right-handedness in the fossil record. J. Hum. Evol. 100, 65–72.
Gallotti, R., Mussi, M., 2015. The unknown Oldowan: ~1.7-million-year-old standardized obsidian small tools from Garba IV, Melka Kunture, Ethiopia. PLoS ONE 10, e0145101.
Gibbon, R.J., Rayne, T., Sutton, M.B., Heaton, J.L., Kuman, K., Clarke, R.J., Brain, C.K., Granger, D.E., 2014. Quaternary geochronology cosmogenic nuclide burial dating of hominin-bearing Pleistocene cave deposits at Swartkrans, South Africa. Quat. Geochron. 24, 10–15.
Gibson, L.J., 1985. The mechanical behaviour of cancellous bone. J. Biomech. 18, 317–328.
Gosman, J.H., Stout, S.D., Larsen, C.S., 2011. Skeletal biology over the life span: a view from the surfaces. Am. J. Phys. Anthropol. 146, 86–98.
Grine, F.E., 2005a. Early *Homo* at Swartkrans, South Africa: a review of the evidence and an evaluation of recently proposed morphs. S. Afr. J. Sci. 101, 43–52.
Grine, F.E., 2005b. Enamel thickness of deciduous and permanent molars in modern *Homo sapiens*. Am. J. Phys. Anthropol. 126, 14–31.
Herries, A.I.R., Curnoe, D., Adams, J.W., 2009. A multi-disciplinary seriation of early *Homo* and *Paranthropus* bearing palaeocaves in southern Africa. Quat. Internat. 202, 14–28.
Hlusko, L.J., Reiner, W.B., Njau, J.K., 2015. A one-million-year-old hominid distal ulna from Olduvai Gorge, Tanzania. Am. J. Phys. Anthropol. 158, 36–42.
Hoffman, J.W., de Beer, F.C., 2012. Characteristics of the Micro-Focus X-ray tomography facility (MIXRAD) at Necsa in South Africa. In: 18th World Conference on non-destructive testing, Durban, South Africa.
Kappelman, J., Ketcham, R.A., Pearce, S., Todd, L., Akins, W., Colbert, M.W., Feseha, M., Maisano, J.A., Witzel, A., 2016. Perimortem fractures in Lucy suggest mortality from fall out of tall tree. Nature 537, 503–507.
Kivell, T.L., 2016. A review of trabecular bone functional adaptation: what have we learned from trabecular analyses in extant hominoids and what can we apply to fossils? J. Anat. 228, 569–594.
Kono, R.T., 2004. Molar enamel thickness and distribution patterns in extant great apes and humans: new insights based on a 3-dimensional whole crown perspective. Anthropol. Sc. 112, 121–146.
L'Abbé, E.N., Loots, M., Meiring, J.H., 2005. The Pretoria bone collection: a modern South African skeletal sample. Homo 56, 197–205.
Lague, M.R., 2014. The pattern of hominin postcranial evolution reconsidered in light of size-related shape variation of the distal humerus. J. Hum. Evol. 75, 90–109.
Lague, M.R., 2015. Taxonomic identification of Lower Pleistocene fossil hominins based on distal humeral diaphyseal cross-sectional shape. PeerJ 3, e1084.
Lague, M.R., Jungers, W.L., 1996. Morphometric variation in Plio-Pleistocene hominid distal humeri. Am. J. Phys. Anthropol. 101, 401–427.
Lague, M.R., Menter, C.G., 2017. DNH 32: a distal humerus of *Paranthropus robustus* from Drimolen, South Africa. Am. J. Phys. Anthropol. 162, S64 (255, abstract).
Lieberman, D.E., Polk, J.D., Demes, B., 2004. Predicting long bone loading from cross-sectional geometry. Am. J. Phys. Anthropol. 123, 156–171.
Lovejoy, C.O., Cohn, M.J., White, T.D., 1999. Morphological analysis of the mammalian postcranium: a developmental perspective. Proc. Nat. Acad. Sc. USA 96, 13247–13252.
Macchiarelli, R., Bondioli, L., Debénath, A., Mazurier, A., Tournepiche, J.F., Birch, W., Dean, M.C., 2006. How Neanderthal molar teeth grew. Nature 444, 748–751.
Macchiarelli, R., Bondioli, L., Galichon, V., Tobias, P.V., 1999. Hip bone trabecular architecture shows uniquely distinctive locomotor behaviour in South African australopithecines. J. Hum. Evol. 36, 211–232.
Martin, L.B., 1985. Significance of enamel thickness in hominoid evolution. Nature 314, 260–263.
Mazurier, A., Nakatsukasa, M., Macchiarelli, R., 2010. The inner structural variation of the primate tibial plateau characterized by high-resolution microtomography. Implications for the reconstruction of fossil locomotor behaviours. C.R. Palevol 9, 349–359.
McHenry, H.M., Brown, C.C., 2008. Side steps: the erratic pattern of hominin postcranial change through time. J. Hum. Evol. 55, 639–651.
Meyer, F., Beucher, S., 1990. Morphological segmentation. J. Vis. Comm. Image Represent. 1, 21–46.

Middleton, K.M., Shubin, C.E., Moore, D.C., Carter, P.A., Garland, T., Swartz, S.M., 2008. The relative importance of genetics and phenotypic plasticity in dictating bone morphology and mechanics in aged mice: evidence from an artificial selection experiment. Zoology 111, 135–147.

Morgan, L.E., Renne, P.R., Kieffer, G., Piperno, M., Gallotti, R., Raynal, J.-P., 2012. A chronological framework for a long and persistent archaeological record: Melka Kunture, Ethiopia. J. Hum. Evol. 62, 104–115.

Nadell, J.A., Shaw, C.N., 2015. Phenotypic plasticity and constraint along the upper and lower limb diaphyses of *Homo sapiens*. Am. J. Phys. Anthropol. 159, 410–422.

Olejniczak, A.J., Smith, T.M., Feeney, R.N., Macchiarelli, R., Mazurier, A., Bondioli, L., Radovčić, J., 2008. Dental tissue proportions and enamel thickness in Neandertal and modern human molars. J. Hum. Evol. 55, 12–23.

Patterson, B., Howells, W., 1967. Hominid humeral fragment from early Pleistocene of northwestern Kenya. Science 156, 64–66.

Pearson, O.M., Lieberman, D.E., 2004. The aging of Wolff's law: ontogeny and responses to mechanical loading in cortical bone. Yearb. Phys. Anthropol. 47, 63–99.

Pickering, T.R., Kramers, J.D., Hancox, P.J., de Ruiter, D.J., Woodhead, J.D., 2011. Contemporary flowstone development links early hominin bearing cave deposits in South Africa. Earth Planet. Sci. Lett. 306, 23–32.

Puymerail, L., 2011. Caractérisation de l'endostructure et des propriétés biomécaniques de la diaphyse fémorale : la signature de la bipédie et la reconstruction des paléo-répertoires posturaux et locomoteurs des Hominines. (PhD dissertation). Museum national d'histoire naturelle, Paris.

Puymerail, L., 2013. The functionally-related signatures characterizing the endostructural organisation of the femoral shaft in modern humans and chimpanzee. C.R. Palevol 12, 223–231.

Puymerail, L., Bondioli, L., Engda, B., Mazurier, A., Macchiarelli, R., 2014. The Early Pleistocene human distal humerus from Gombore I, Melka Kunture (Upper Awash basin, Ethiopia). Cortical bone topography and structural organization. Int. Symp. The Afr. Hum. Foss. Rec., 15–16 (Toulouse, http://www.tahfr.cnrs.fr, abstract).

Puymerail, L., Ruff, C.B., Bondioli, L., Widianto, H., Trinkaus, E., Macchiarelli, R., 2012. Structural analysis of the Kresna 11 *Homo erectus* femoral shaft (Sangiran, Java). J. Hum. Evol. 63, 741–749.

Rein, T.R., Harrison, T., Carlson, K.J., Harvati, K., 2017. Adaptation to suspensory locomotion in *Australopithecus sediba*. J. Hum. Evol. 104, 1–12.

Rhodes, J.A., Knüsel, C.J., 2005. Activity-related skeletal change in medieval humeri: cross-sectional and architectural alterations. Am. J. Phys. Anthropol. 128, 536–546.

Roerdink, J., Meijster, A., 2000. The watershed transform: definitions, algorithm and parallelization strategies. Fundam. Informat. 41, 178–228.

Ruff, C.B., 2002. Long bone articular and diaphyseal structure in Old World monkeys and apes. I. Locomotor effects. Am. J. Phys. Anthropol. 119, 305–342.

Ruff, C.B., 2008. Biomechanical analyses of archaeological human skeletons. In: Katzenberg, M.A., Saunders, S.R. (Eds.), Biological anthropology of the human skeleton. Alan R. Liss, New York, pp. 183–206.

Ruff, C.B., Burgess, M.L., Ketcham, R.A., Kappelman, J., 2016. Limb bone structural proportions and locomotor behavior in A.L. 288-1 ("Lucy"). PLoS ONE 11 (11), e0166095.

Ruff, C.B., Holt, B., Trinkaus, E., 2006. Who's afraid of the big bad Wolff? Wolff's law and bone functional adaptation. Am. J. Phys. Anthropol. 129, 484–498.

Ryan, T.M., Shaw, C.N., 2013. Trabecular bone microstructure scales allometrically in the primate humerus and femur. Proc. Roy. Soc. B 280, 20130172.

Ryan, T.M., Shaw, C.N., 2015. Gracility of the modern *Homo sapiens* skeleton is the result of decreased biomechanical loading. Proc. Nat. Acad. Sc. USA 112, 372–377.

Ryan, T.M., Sukhdeo, S., 2016. KSD-VP-1/1: Analysis of the postcranial skeleton using high-resolution computed tomography. In: Haile-Selassie, Y., Su, D.F. (Eds.), The Postcranial Anatomy of *Australopithecus afarensis*: new insights from KSD-VP-1/1. Vertebrate paleobiology and paleoanthropology Series. Springer, Dordrecht, pp. 39–62.

Senut, B., 1979. Comparison des hominidés de Gomboré IB et de Kanapoi : deux pièces du genre *Homo* ? Bull. Mem. Soc. Anthropol. Paris 6, 111–117.

Senut, B., 1981a. Outlines of the distal humerus in hominoid primates: application to some Plio-Pleistocene hominids. In: Chiarelli, B., Corruccini, R.S. (Eds.), Primate evolutionary biology. Springer-Verlag, Berlin, pp. 81–92.

Senut, B., 1981b. Humeral outlines in some hominoid primates and in Plio-Pleistocene hominids. Am. J. Phys. Anthropol. 56, 275–283.

Skinner, M.M., Kivell, T.L., Potze, S., Hublin, J.-J., 2013. Microtomographic archive of fossil hominin specimens from Kromdraai B, South Africa. J. Hum. Evol. 64, 434–447.

Smith-Adaline, E.A., Volkman, S.K., Ignelzi Jr., M.A., Slade, J., Platte, S., Goldstein, S.A., 2004. Mechanical environment alters tissue formation patterns during fracture repair. J. Orthop. Res. 22 (5), 1079–1085.

Spoor, F., Zonneveld, F., Macho, G., 1993. Linear measurements of cortical bone and dental enamel by computed tomography: applications and problems. Am. J. Phys. Anthropol. 91, 469–484.

Stauber, M., Müller, R., 2006. Volumetric spatial decomposition of trabecular bone into rods and plates: a new method for local bone morphometry. Bone 38, 475–484.

Straus, W.L., 1948. The humerus of *Paranthropus robustus*. Am. J. Phys. Anthropol. 6, 285–313.

Susman, R.L., 1989. New hominid fossils from the Swartkrans Formation (1979–1986 excavations), postcranial specimens. Am. J. Phys. Anthropol. 79, 451–474.

Susman, R.L., de Ruiter, D., Brain, C.K., 2001. Recently identified postcranial remains of *Paranthropus* and early *Homo* from Swartkrans Cave, South Africa. J. Hum. Evol. 41, 607–629.

Tamrat, E., Thouveny, N., Taieb, M., Brugal, J.-P., 2014. Magnetostratigraphic study of the Melka Kunture archaeological site (Ethiopia) and its chronological implications. Quat. Internat. 343, 5–16.

Thackeray, J.F., De Ruiter, D.J., Berger, L.R., Van Der Merwe, N.J., 2001. Hominid fossils from Kromdraai: a revised list of specimens discovered since 1938. Ann. Transv. Mus. 38, 43–56.

Trinkaus, E., Ruff, C.B., 2012. Femoral and tibial diaphyseal cross-sectional geometry in Pleistocene Homo. Paleo. Anthropol. 2012, 13–62.

Volkman, S.K., Galecki, A.T., Burke, D.T., Paczas, M.R., Moalli, M.R., Miller, R.A., Goldstein, S.A., 2003. Quantitative trait loci for femoral size and shape in a genetically heterogeneous mouse population. J. Bone Miner. Res. 18, 1497–1505.

Volpato, V., Couture, C., Macchiarelli, R., Vandermeersch, B., 2011. Endostructural characterization of the Regourdou 1 Neanderthal proximal arm: bilateral asymmetry and handedness. In: Condemi, S., Weniger, G.-C. (Eds.), Continuity and discontinuity in the peopling of Europe. Vertebrate paleobiology and paleoanthropology series. Springer, New York, pp. 175–178.

Volpato, V., Macchiarelli, R., Guatelli-Steinberg, D., Fiore, I., Bondioli, L., Frayer, D.W., 2012. Hand to mouth in a Neandertal: right handedness in Regourdou 1. PLoS ONE 7, e43949.

Vrba, E., 1981. The Kromdraai australopithecine site revisited in 1980: recent investigations and results. Ann. Transv. Mus. 33, 17–60.

Vrba, E.S., 1985. Early hominids in southern Africa: updated observations on chronological and ecological background. In: Tobias, P.V. (Ed.), Hominid evolution: past, present and future. Alan R. Liss, New York, pp. 195–200.

Wallace, I.J., Middleton, K.M., Lublinsky, S., Kelly, S.A., Judex, S., Garland, T., Demes, B., 2010. Functional significance of genetic variation underlying limb bone diaphyseal structure. Am. J. Phys. Anthropol. 143, 21–30.

Wallace, I.J., Tommasini, S.M., Judex, S., Garland Jr., T., Demes, B., 2012. Genetic variations and physical activity as determinants of limb bone morphology: an experimental approach using a mouse model. Am. J. Phys. Anthropol. 148, 24–35.

White, T.D., Black, M.T., Folkens, P.A., 2012. Human osteology, third ed. Academic Press, San Diego.

Wilson, L.A.B., Humphrey, L.T., 2015. A virtual geometric morphometric approach to the quantification of long bone bilateral asymmetry and cross-sectional shape. Am. J. Phys. Anthropol. 158, 541–556.

Zanolli, C., Dean, M.C., Assefa, Y., Bayle, P., Braga, J., Condemi, S., Endalamaw, M., Engda Redae, B., Macchiarelli, R., 2016. Structural organization and tooth development in a *Homo* aff. *erectus* juvenile mandible from the Early Pleistocene site of Garba IV at Melka Kunture, Ethiopian highlands. Am. J. Phys. Anthropol., http://dx.doi.org/10.1002/ajpa.23135.